Aggregation Processes of Hydrophobically Modified Polyethylene Oxide

Kee Wook Paeng, Bum-Sung Kim,† Eung-Ryul Kim, and Daewon Sohn*

Department of Chemistry, Hanyang Univ., Haengdang Dong 17, Seoul 133-791, Korea
†Korea Chemical Co., Ltd., San 1-9 Mabook Ri, Kyunggi Do 449-910, Korea
Received January 20, 2000

Aggregation of hydrophobically end-capped poly(ethylene oxide)s: HEURs, denoted as $C_8EO_{380}C_8$, $C_{12}EO_{600}C_{12}$, and $C_{18}EO_{860}C_{18}$, are described using static fluorescence, dynamic light scattering, and atomic force microscope (AFM) techniques. The CAC (critical aggregation concentration) was determined by comparing two fluorescent peaks which were influenced by the polarity of the probe dye molecules, pyrene. The aggregation occurs in concentrations higher than 10 g/L of $C_8EO_{380}C_8$ and the CAC decreases by increasing the side chain length. The dynamic light scattering experiment shows fast mode and slow mode decays, and both are diffusive. The fast mode does not depend on the concentration, but the slow mode shows concentration dependence influenced by the formation of an aggregated structure. The hydrophobic end groups effect more dominantly than the main chains for the formation of HEUR micelles. By increasing the concentration, the HEUR micelles change their structure from spheres to rodlike micelles, and finally make fused structures, which were visualized with atomic force microscopy.

Introduction

The water soluble polymers with hydrophobic end groups play an important role as viscosity modifiers in water borne technologies such as paints, inks, and cosmetics.[1,2] The associated thickener increases the solution viscosity, and its rheological behavior is essential for the ingredient formulation.[3] The associated mechanism of the water-soluble polymer began with systematic studies on a series of well-defined HEUR (hydrophobic ethoxylated urethane) polymers.[4] Rheological measurements were focused in the early stages.[5-8] However, recently fundamental studies have been conducted by several research groups using an extensive series of methods including fluorescent probe experiment,[9-17] pulsed gradient spin echo (PGSE) nuclear magnetic resonance (NMR),[18-21] dynamic light scattering,[9,10,22-25] and small-angle scattering (SAXS, SANS).[26,27] From a fundamental point of view, the molecules with low polydispersity and direct modification of the hydroxyl group of poly(ethylene oxide) are more interesting. The synthesis processes of these molecules have been recently introduced by Alami *et al.* and characterized by NMR, UV, and SEC.[27,28]

Associating polymers containing hydrophobic side chains and hydrophilic main chains are similar to surfactant molecules. At low concentrations the hydrophobic side chains of the polymer are assembled inside the micelle, and the hydrophilic main chains make a loop and generate a flower type structure.[29-31] When the concentration exceeds the CAC, the intercrossing of the PEO chains takes place and viscosity rises abruptly. However, models of micelle connectivity by superbridges, superloops, or dangling ends are still controversial. Here, we suggest that the end group effect is more dominant than the main chain contribution for the formation of the micelle of HEUR. The polymer micelles with three different PEO contents and three different side chain length of the associated polymers were used to provide the aggregation model.

Experimental Section

Associated polymers have been kindly provided by prof. E. Kumacheva at the Univ. of Toronto, Canada. The molecular weight of three different molecules which is end-capped with octyl (C=8), dodecyl (C=12) and octadecyl (C=18) alkyl chain, respectively, are determined by GPC and denoted by $C_8EO_{380}C_8$ (Mw: 16,700, Mw/Mn: 1.18), $C_{12}EO_{600}C_{12}$ (Mw: 26,200, Mw/Mn: 1.22), and $C_{18}EO_{860}C_{18}$ (Mw: 37,650, Mw/Mn: 1.27). The weight ratio of these side chains to the main chain PEO is 1.35, 1.29, and 1.34%, respectively.

Fluorescence spectra were measured on an ISS PC1 photon counting spectro-fluorometer between 350 and 450 nm. Pyrene was used as a probe at 6×10^{-7} M and with excited wavelength at 334 nm. Pyrene used in the fluorescence studies was purchased from Aldrich and purified by a process in the reference.[12] The peak position is not affected by the solvent type, but the intensity of the peak is influenced by the solvent polarity.[32,33] Instrumental error to read the intensity is within 3%.

Dynamic light scattering measurements were performed using a UNIPHASE He-Ne laser operating at 632.8 nm. The maximum operating power of the laser was 30 mW. The detector optics employed optical fibers coupled to an ALV/SO-SIPD/DUAL detection unit which employed an EMI PM-28B power supply and ALV/PM-PD preamplifier/discriminator. The signal analyzer was an ALV-5000/E/WIN multiple tau digital correlator with 288 exponentially spaced channels. Its minimum real sampling time is 10^{-6} s and a maximum of about 100s. A lens with a focal length of 200 mm narrowed the incident beam to reduce the thermal lensing effect and to increase the coherence area. The scattered beam passed through two pin holes (diameter 400 and 400 μm, respectively) before reaching the PMT. A scattering cell (10 mm diameter cylindrical) was placed in a temperature controlled bath of index matching liquid, toluene. All of the experiments were performed at 25 ± 0.1 °C.

An atomic force microscope, Park Scientific Instrument, Autoprobe CP, equipped with a Si_3N_4 tip was used to observe the self-assembled micelle on a solid surface. The spring constant was 0.4 N/m and the images were obtained in contact mode. Scan rates were varied from 2 to 4 Hz. All samples were examined at an ambient temperature. The self-assembled samples were prepared by soaking a clean mica piece into the HEUR solution for several minutes. The images presented in this work were obtained at several different spots of the sample.

Results and Discussion

The fluorescence emission spectrum exhibits five peaks denoted I-V. Figure 1(a) shows the fluorescence emission spectrum of pyrene in water. Polarity sensitive dye like pyrene provides information about the hydrophobicity of the dye environment in the micelle. It is known that: 1) the intensity of peak 1 (at 372 nm) is weak in nonpolar solvent and strong in polar solvent, 2) the I/III ratio is 1.8-1.9 in water and reaches 0.6 in nonpolar solvent.[32,33] Pyrene is mainly hydrophobic probe and its solubility in water is very low (2-3 μM). In the presence of micelles, pyrene is preferentially diffuse into the hydrophobic domain of the micelles. Typical I/III value for aqueous micelle system is 1.1-1.2, implying the pyrene is located in the surface region of the micelle hydrocarbon core. The intensity of the peak changes by adding HEUR polymers in the pyrene solution as in Figure 1(b), in which the HEUR, $C_{12}EO_{600}C_{12}$, concentration is 21.30 g/L.

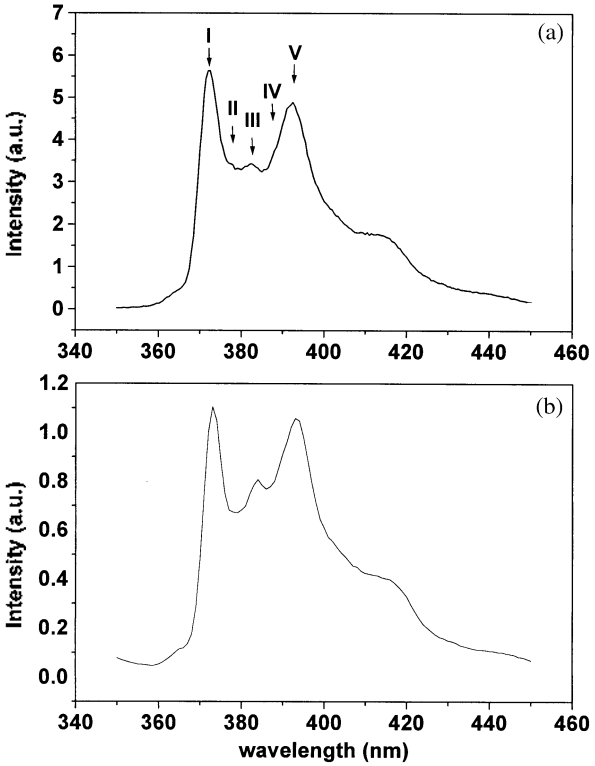

Figure 1. (a) A fluorescence emission spectrum of the pyrene in water, and (b) in HEUR solution of 21.30 g/L.

The I/III ratio of HEUR spectra was measured as a function of polymer concentration. Figure 2 shows the I/III ratio of the fluorescence emission spectrum of pyrene in $C_8EO_{380}C_8$, $C_{12}EO_{600}C_{12}$, and $C_{18}EO_{860}C_{18}$ solutions as a function of HEUR concentration, respectively.

The transition of I/III ratio of $C_8EO_{380}C_8$ in Figure 2(a) occurs at a relatively high concentration, ~10 g/L, compared with $C_{12}EO_{600}C_{12}$ and $C_{18}EO_{860}C_{18}$ which shows the transition at lower concentrations, ~1 g/L and ~10^{-2} g/L, respectively. The I/III ratios of $C_8EO_{380}C_8$ and $C_{12}EO_{600}C_{12}$ decrease over an order of decay from 10 g/L to 100 g/L concentration region. For the $C_{18}EO_{860}C_{18}$ the I/III transition occurs over broader concentration range, from 10^{-2} g/L to 2 g/L. Generally, the CAC is located on the inflection point of the I/III curve and their inflection points are 16.16, 3.33, and 0.017 g/L for the $C_8EO_{380}C_8$, $C_{12}EO_{600}C_{12}$, and $C_{18}EO_{860}C_{18}$, respectively. The I/III ratio decreases and reaches the flat

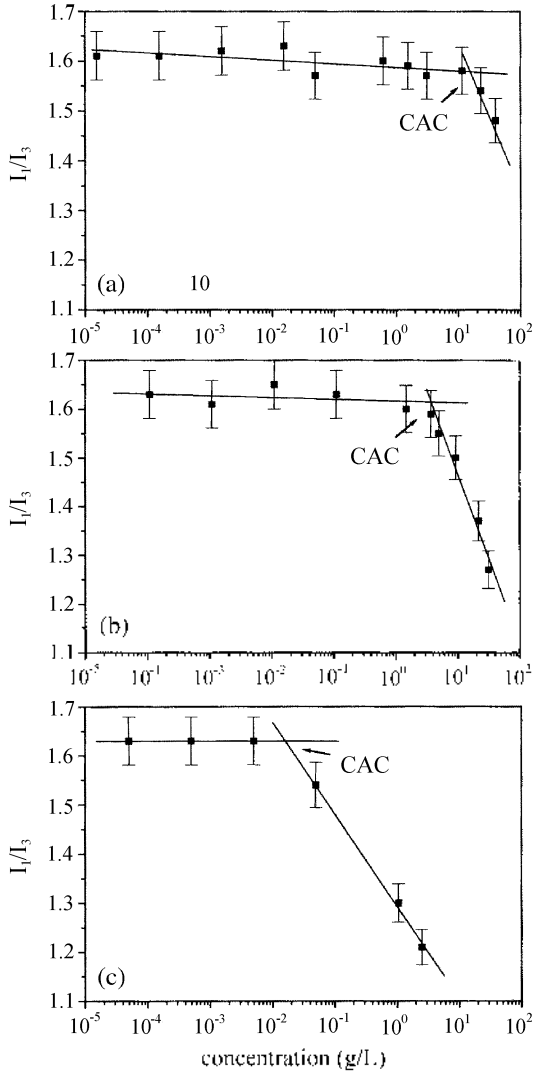

Figure 2. The I/III ratio of fluorescence emission spectrum intensity of three HEURs. (a) $C_8EO_{380}C_8$, (b) $C_{12}EO_{600}C_{12}$, and (c) $C_{18}EO_{860}C_{18}$, by changing the concentration. The error bar indicates 3% experimental error.

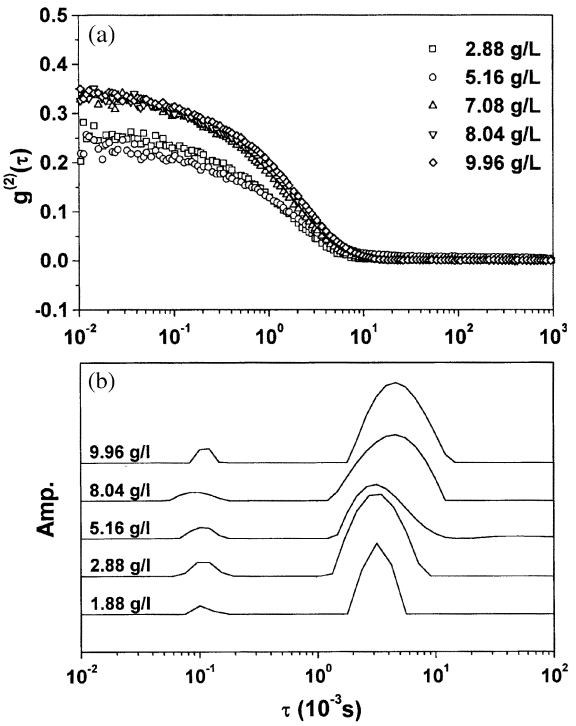

Figure 3. (a) The intensity-intensity correlation function, $g^{(2)}(\tau)$, and (b) the distributions of relaxation times obtained by inverse Laplace transformation, scattering angle 60° at various concentration of $C_{12}EO_{600}C_{12}$.

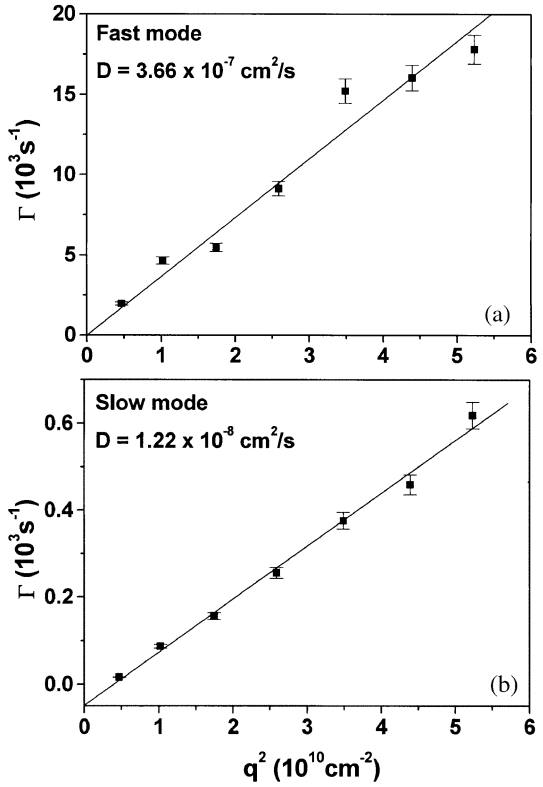

Figure 4. (a) Angular dependence of the fast mode and (b) the slow mode from one of the samples, 16.4 g/L of $C_{12}EO_{600}C_{12}$.

region (data not shown) where the hydrophobic domains are relatively small in the solution. The difference between the transitions strongly depends on the PEO contents and lengths of the hydrophobic end groups of the HEURs. Long range distribution of the I/III ratio in $C_{18}EO_{860}C_{18}$ indicates that longer PEO chain makes broad distribution of the polarity of the pyrene molecules, which also implies the more flexible micelle structure for the long ethylene oxide chains, $C_{18}EO_{860}C_{18}$.

Figure 3 shows the intensity-intensity correlation function, $g^{(2)}(\tau)$, at a scattering angle of 60° of various concentration of $C_{12}EO_{600}C_{12}$. The scattered intensity was hardly detected below CAC and the concentrations in Figure 3 are near the CAC.

The intensity-intensity correlation function:

$$g^{(2)}(\tau) = \lim_{T\to\infty} \frac{1}{2T}\int_{-T}^{T} I(t)I(t-\tau)dt$$

$$= B(1 + f\,|\,g^{(1)}(\tau)|^2)$$

Here, τ is the lag time, B is the baseline, and f is an instrumental parameter depending mostly on the number of coherence areas detected. The normalized first order correlation function is given by a single exponential, $g^{(1)}(\tau) = \exp(-\Gamma\tau)$, where Γ is the relaxation rate. Distributions of relaxation times were obtained by inverse Laplace transformation using the algorithm CONTIN.[34] The small-fast mode and the large-slow mode are clearly indicated in Figure 3(b) and both modes are proportional to the angle. Angular dependence of these modes in Figure 4(a) and (b) indicates that both modes are diffusive. The fast mode is a result of single molecular diffusion or small oligomeric aggregations and the slow mode is due to the agglomerated micellar structure. The diffusion coefficient of the fast mode and the slow mode are calculated from the gamma *vs.* q^2 plot, $D = \Gamma/q^2$, where D is the diffusion coefficient, q is the magnitude of the scattering vector, $q = 4\pi n_0 \sin(\theta/2)/\lambda_0$, n_0 is the refractive index of solvent, λ_0 is the wavelength in vacuum, and θ is the scattering angle. The deviation to fit the correlation function is indicated by error bar in Figure 4 (a) and (b). The corresponding hydrodynamic radii, 5.8 nm and 175.1 nm, respectively, are deduced from $R_h = kT/(6\pi\eta D)$, where k is Boltzmann constant and η is solvent viscosity. By increasing the concentration, the fast mode remains at the same position of the distribution function, but the slow mode shifts to the longer relaxation time. HEUR with longer ethylene oxides chains, $C_{18}EO_{860}C_{18}$, also shows two diffusive modes.

The I/III results show a range of extensive formation of micellar aggregations. The fluorescence quenching and DLS measurements mark the size and the aggregation process in more distinct ways. At very low concentrations, most polymer molecules are free or in small oligomeric aggregations. Fluorescence and light scattering measurements cannot distinguish between these forms. However, a series of samples with different lengths of main chains and hydrophobic end groups suggest a driving factor to form the HEUR micelle. The recently discussed models of free energy changes with the formation of loops of an end-modified polymer can be

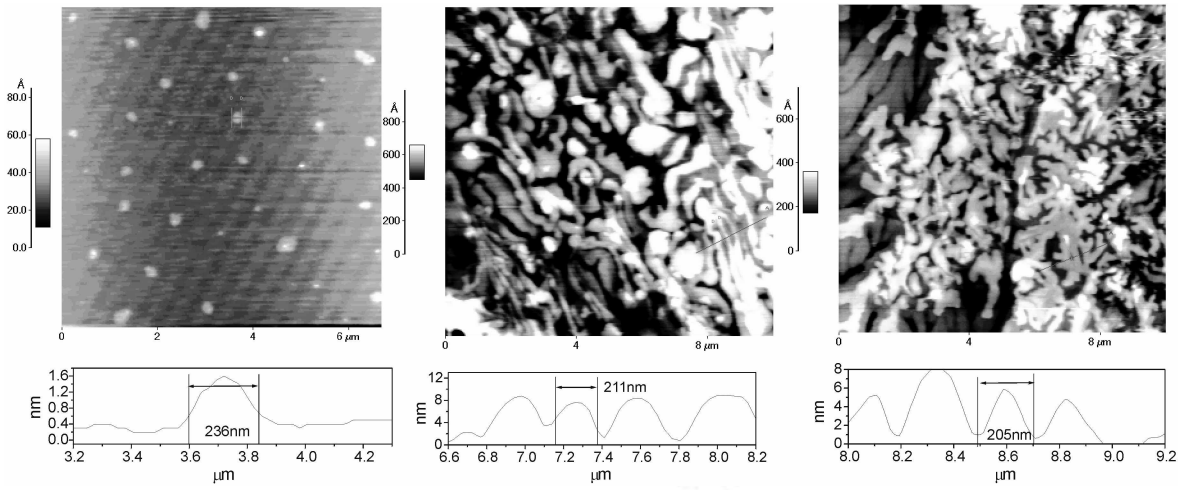

Figure 5. AFM images of HEURs, $C_{18}EO_{860}C_{18}$, self-assembled on mica surface from solution in (a) 1.0 g/L, (b) 3.0 g/L, and (c) 30 g/L. The time of exposure is 30 min.

applied for the systems, in which; 1) there is a loss of entropy when the polymer chain is back-folded, and 2) there is a gain in hydrophobic free energy when the chains associated. Several authors proposed the gain of free energy on association of the tails and the loss of entropy of the Gaussian chains.[9] In the cases of decreased lengths of the PEO chain or longer alkyl groups, loops would become more favorable. In our case, in spite of the long PEO chain, the gain in hydrophobic energy of $C_{18}EO_{860}C_{18}$ to form more favorable micellar structures than those of the short alkyl chain ended HEUR. The loop formation would strongly depend on the energetic contributions of the hydrophobic side chains. But as mentioned above, the flexibility and size of the micelle would depend on the size of PEO chain.

Since the open association model proposed by Maechling-Strasser,[23] in which the fundamental building blocks were unassociated polymer chains, Winnik suggested a closed association model.[11] Winnik's rosette-like micelle model is that the individual polymer chains associated to form micelles of a well defined structure, but these micelles undergo secondary association to form clusters. Nystrom and Hansen suggest a fractal-like structure with relaxation processes by DLS and PGSE-NMR.[21] At high polymer concentrations, they suggest the polymer chains undergo a series of loop-bridge, bridge-bridge, and bridge-loop steps.

To visualize the micelle structure of the HEUR polymers, we transfer the micelle onto the solid surface and observed it through the atomic force microscope. Figure 5 shows the AFM images of the HEUR ($C_{18}EO_{860}C_{18}$) micelles formed at different concentration solutions by self-assembling on the mica surface.

The layer of micelles is strongly adsorbed on the mica surface because the AFM images after scanning of contact mode does not show any disruption of the micellar structure. Adsorption from a dilute solution, 1.0 g/L of HEUR, produces spherical micellar particles as in Figure 5(a). The average height is ~2.0 nm, while the diameter of the sphere varies from 137 nm to 255 nm. As the HEUR concentration increases to 3.0 g/L, fused HEUR structures with stripes and circles were observed. The thickness of a fine stripe is 211 nm, which is the same as the diameter of the spherical micelle. It is speculated that the stripes and spheres fused together and generate huge rodlike structures with the length of several μm. The huge rodlike morphology is preserved upon the breakage of the structure by increasing the concentration up to 3.0 g/L. Figure 5 (c) shows the self-assembly of HEUR prepared at a high concentration, 30 g/L. The surface coverage increased and a highly defused structure was created by bridging both in the vertical and horizontal directions.

In conclusion, the end groups effect more seriously than the long main chains to form the HEUR micelle. The flower-

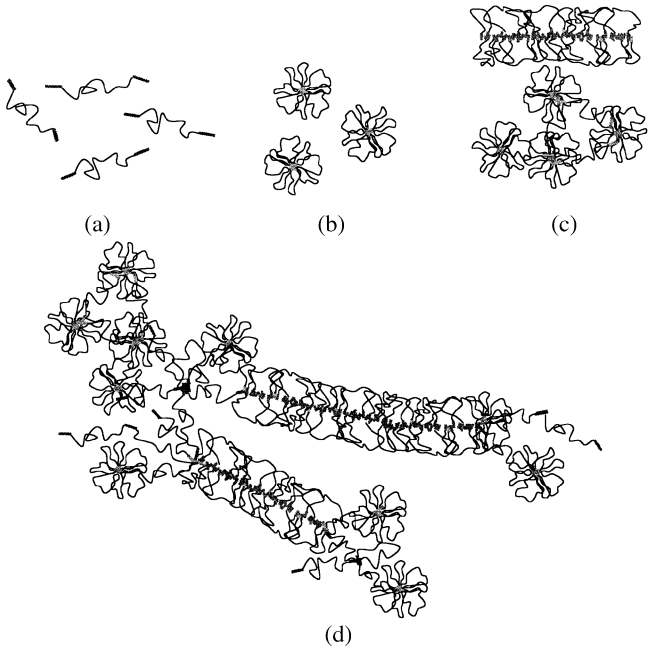

Figure 6. Schematic representation of the formation of aggregated HEURs. (a) at low concentration, (b) at critical micelle concentration, (c) and (d) after cac.

like micelle in the dilute solution expands and generates the rodlike structure by increasing the concentration. Then the micelles diffuse each other and generate the large fractal-like structure in high concentrations. These were not clear in the previous light scattering and fluorescence studies. Figure 6 represents the schematic model for the formation of HEUR micelle by concentration increments; HEUR molecules (a) freely move in low concentration solutions, (b) generate spherical micelles by increasing the concentration, (c) diffuse each other and generate the rodlike micelle, and (d) interconnect the rod-like micelles and generate huge fractal structures.

Acknowledgment. D. S. is indebted to Prof. E. Kumacheva in the Department of Chemistry at University of Toronto. This work was supported by the research fund of Hanynag University in 1999.

References

1. Schaller, E. In *Advances in Emulsion Polymerization and Latex Techenology*; 20th Annual Short Course, 1989; Vol. 2, Lecture No. 12.
2. Nah, J. W.; Jeong, Y. I.; Cho, C. S. *Bull. Korean Chem. Soc.* **1998**, *19*(9), 962.
3. *Polymer as Rheology Modifier*; Schultz, D. N., Glass, J. E., Eds.: Advances in Chemistry Series NO. 462: American Chemical Society Symposium: Washington, DC, 1991.
4. Jenkins, R. D. *Ph.D. Dissertation*: Lehigh University: Bethlehem, PA, 1990.
5. Karunasena, A.; Glass, J. E. *Prog. Org. Coat.* **1989**, *17*, 301.
6. *Polymer in Aqueous Media*; Glass, J. E., Ed.; Advances in Chemistry 233; American Chemical Society: Washington, DC, 1989.
7. *The Function of Associative Thickeners in Water-borne Paints*; Hudén, M., Sjöblom, E., Bröström, P., Eds.; XXI Fatipec Congress: Amsterdam, 1992.
8. Huldén, M. *Colloid Surf. A* **1994**, *82*, 263.
9. Alami, E.; Almgren, M.; Brown, W.; Francois, J. *Macromolecules* **1996**, *29*, 2229.
10. Alami, E.; Almgren, M.; Brown, W. *Macromolecules* **1996**, *29*, 5026.
11. Xu, B.; Yekta, A.; Li, L.; Masonmi, Z.; Winnik, M. A. *Colloids and Surfaces A* **1996**, *112*, 239.
12. Yekta, A.; Duhamel, J.; Brochard, P.; Adiwidjaja, H.; Winnik, M. A. *Macromolecules* **1993**, *26*, 1829.
13. Yekta, A.; Duhamel, J.; Adiwidjaja, H.; Winnik, M. A. *Macromolecules* **1995**, *28*, 956.
14. Wang, Y.; Winnik, M. A. *Langmuir* **1990**, *6*, 1437.
15. Hansson, P.; Almegren, M. *Langmuir* **1994**, *10*, 2115.
16. Yeo, S. I.; Woo, K. W. *Bull. Korean Chem. Soc.* **1998**, *19*(10), 1054.
17. Yekta, A.; Duhamel, J.; Adiwijaja, H.; Brochard, P.; Winnik, M. A. *Langmuir* **1993**, *9*, 881.
18. Rao, B.; Uemura, Y.; Dyke, L.; Macdonald, P. M. *Macromolecules* **1995**, *28*, 531.
19. Persson, K.; Abrahamsén, S.; Persson, K.; Stilbs, P.; Hansen, F. K.; Walderhaug, H. *Colloid Polym. Sci.* **1992**, *270*, 465.
20. Walderhaug, H.; Hansen, F. K.; Abrahamsén, S.; Persson, K.; Stilbs, P. *J. Phys. Chem.* **1993**, *97*, 8336.
21. Hansen, F. K.; Nyström, B.; Walderhaug, H. *Macromol. Symp.* **1995**, *92*, 345.
22. Chassenieux, C.; Nicolai, T.; Durand, D. *Macromolecules* **1997**, *30*, 4952.
23. Maechling-Strasser, C.; François, J.; Clouet, F.; Tripette, C. *Polymer* **1992**, *33*, 627.
24. Maechling-Strasser, C.; Clouet, F.; François, J. *Polymer* **1992**, *33*, 1021.
25. Nyström, B.; Walderhaug, H.; Hansen, F. K. *J. Phys. Chem.* **1993**, *97*, 7743.
26. François, J.; Maitre, S.; Rawiso, M.; Sarazin, D.; Beinert, G.; Isel, F. *Colloids Surf. A* **1996**, *112*, 251.
27. *Hydrophobic Polymers*; Alami, E., Rawiso, M., Isel, F., Beinert, G., Binana-Limbelé, W., François, J., Eds.: Advances in Chemical Series 248; American Chemical Society: Washington, DC, 1995; Chapter 18.
28. François, J. *Prog. Org. Coat.* **1994**, *24*, 67.
29. Semenov, A. N.; Joanny, J. F.; Khokhlov, A. R. *Macromolecules* **1995**, *28*, 1066.
30. Borisov, O. V.; Halperin, A. *Macromolecules* **1996**, *29*, 2612.
31. Halperin, A. *Macromolecules* **1987**, *20*, 2943.
32. *The Chemistry of Excitation at Interfaces*; Thomas, J. K.; Ed.; ACS Monograph NO. 181; American Chemical Society: Washington, DC, 1984.
33. Kalyanasundaran, K.; Thomas, J. K. *J. Am. Chem. Soc.* **1977**, *99*, 2039.
34. Provencher, S. W. *Comp. Phys.* **1982**, *27*, 229.